Eur. Phys. J. D **15**, 127–135 (2001)

THE EUROPEAN PHYSICAL JOURNAL D

EDP Sciences

Quantum structures in traveling-wave spontaneous parametric down-conversion

E. Brambilla[1,a], A. Gatti[1], L.A. Lugiato[1], and M.I. Kolobov[2]

[1] Dipartimento di Scienze CC.FF.MM.,Università dell'Insubria, Via Valleggio 16, 22100 Como, Italy
[2] Laboratoire de Physique des Lasers, Atomes et Molécules, Université des Sciences et Technologies de Lille, Bâtiment P5, 59655 Villeneuve d'Ascq Cedex, France

Received 5 February 2001 and Received in final form 11 April 2001

Abstract. We analyze theoretically spatial structures appearing in the far diffraction zone of the electromagnetic field emitted in the cavityless parametric down-conversion. We investigate in detail the spatial correlation functions of intensity and demonstrate the existence of strong quantum correlations between the regions of the far field symmetrical with respect to the optical axis. Our simplified model allows us to obtain analytical results for some limiting cases. We demonstrate that in the limit of small diffraction and ideal quantum efficiency of photodetection the noise reduction in the photocurrent difference between symmetrical regions in the far diffraction field becomes complete at zero frequency of photocurrent fluctuations.

PACS. 42.50.Dv Nonclassical field states; squeezed, antibunched, and sub-Poissonian states; operational definitions of the phase of the field; phase measurements – 03.67.-a Quantum information – 42.65.-k Nonlinear optics

1 Introduction

Entanglement is one of the most intriguing and profound concepts of quantum mechanics. It leads to fundamental problems such as the Einstein-Poldosky-Rosen (EPR) paradox and violation of the Bell inequalities. Optics, in these respects, has a special position since entangled states of the radiation field can be generated rather easily by exploiting wave-mixing phenomena arising from the nonlinear interaction between light and matter. The nonlinear interaction between waves of different frequencies can be seen at an elementary level as the result of simultaneous absorption or emission of several photons. For example in the case of the second-order parametric process two photons are emitted or absorbed simultaneously. Such processes create a quantum entanglement between different modes of the field in play, and strong quantum correlations can be observed at a mesoscopic or even macroscopic level, since the number of generated photons can be very large.

EPR aspects have been demonstrated for the two-mode squeezed state produced by an optical parametric oscillator as a result of an entanglement in the photon number and phase [1]. A number of novel applications using the peculiar properties of entangled states have been proposed, such as quantum cryptography [2], quantum computation, and quantum teleportation [3]. Until recently quantum correlations arising from entanglement have been investigated mainly in the temporal domain, considering only the interaction between a very small number of modes (typically these modes are selected by a resonant cavity which encloses the nonlinear medium).

However, when the nonlinear interaction involves a large number of transverse modes of the electromagnetic field, quantum correlations can emerge also in the transverse cross-section of the generated beam, *i.e.* in the spatial domain. Nonclassical states of the radiation field which display such spatial entanglement are of great interest for applications, since they allow in principle to process and transmit information in a parallel way [4,5].

The investigation of the spatial aspects of quantum entanglement was carried out initially in the case of nonlinear optical patterns [4] and, more recently, has lead to an approach that now is often called *quantum imaging*. It intends to explore for example, the ultimate limits imposed by quantum mechanics in the detection of fine image details, of sharp edges [6], to improve the image retrieval, resolution [7], and storage by using quantum correlations. Investigations are carried out both at the level of single photon pairs [8] and for intense beams.

Our group has studied spatial entanglement in optical parametric oscillators below threshold [9,10]. More recently we have explored the case in which an image is injected, *via* an appropriate imaging system, into an optical parametric oscillator below threshold or, equivalently, into a cavityless optical parametric amplifier.

[a] e-mail: enrico.brambilla@uninsubria.it

In references [11,12] we have shown that such system can generate two amplified copies of the input image which are strongly entangled one to each other. In this context, the concept of twin images arises as a natural generalization of that of twin beams to the optical fields with a large number of spatial modes.

In this paper we analyze the field generated by traveling-wave spontaneous parametric down-conversion in a $\chi^{(2)}$ crystal. The number of modes in such a system is very large because of its broadband nature in both temporal and spatial domains. For this reason such a system is well-suited to work as an optical imaging system and has been studied in recent experiments [13]. However these experimental works do not exploit the quantum features of the generated field. The first experiment with this specific goal has been performed by Kumar and co-workers [14], who demonstrated the possibility of obtaining *noiseless* amplification for a given spatial frequency, confirming thereby the prediction of [15,16].

The spontaneously down-converted field is generated by the vacuum fluctuations and hence it arises even in the absence of any injected input field (apart from the pump field, of course). This spontaneous radiation can represent a disturbing source of noise when the device works as an amplifier. However, it also displays very interesting quantum correlations. We want to analyze them in the spatial domain, considering the whole multimodal structure of the field.

We study the quantities similar to those considered in [9], *i.e.* the spatial correlation functions of the intensity fluctuations and the fluctuations in the intensity difference between two symmetrical regions of the far field, but we study a single-pass parametric down-conversion instead of a parametric oscillator below threshold investigated in [9]. Because of the simplicity of the cavityless case, it is possible to carry out analytical calculations up to the very end in specific relevant cases and, in general, to obtain final expressions that allow for a quantitative numerical evaluation. In the case of an optical parametric oscillator below threshold, instead, the final expressions contain multiple sums over the Gauss-Laguerre modes [9], which makes numerical calculations very hard beyond a limited region of the parameter space.

In Section 2 we describe our model. The developed multimode theory accounts for the main features of the far-field intensity distribution, as shown in Section 3. The quantum correlations in the far-field intensity distribution are analyzed in Section 4. In Section 5 we show that intensity fluctuations in symmetrical regions of the ring pattern are perfectly correlated, as a consequence of the quantum nature of the generated twin photons in the parametric down-conversion. The conclusion are drown in Section 6.

2 The model

In contrast to the case of an optical parametric oscillator, where cavity mode selection plays an important role, in a single-pass configuration phase matching is the main mechanism that determines the angular spectrum and the spatial structure of the down-converted field. Indeed, for a fixed wave vector of the pump field $\mathbf{k}_\mathrm{p}$, noncollinear phase-matching can generally be fulfilled for a continuous range of frequencies of the signal and the idler modes, ω_s and ω_i, related by the energy conservation law $\omega_\mathrm{s}+\omega_\mathrm{i}=\omega_\mathrm{p}$. In our model the pump field is a monochromatic plane wave. We consider the simplest case of a type-I phase matching, with the signal and the idler waves having the same ordinary polarization, so that their dispersion relation $k(\omega)$ does not depend on the propagation direction. Moreover, we will be interested in the situation when spontaneous down-conversion takes place close to the degenerate frequency $\omega_\mathrm{s}=\omega_\mathrm{p}/2$. Under these assumptions each elementary down-conversion process corresponds to the destruction of a pump photon of frequency ω_p and the simultaneous creation of a pair of photons with frequencies $\omega_\mathrm{s}+\Omega$ and $\omega_\mathrm{s}-\Omega$ (with $\Omega \ll \omega_\mathrm{s}$), and the transverse components of the wave vector equal to $\mathbf{q}$ and $-\mathbf{q}$.

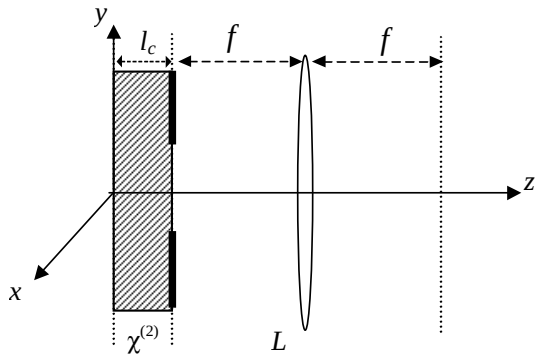

Fig. 1. Scheme of the optical system. Far-field measurements are performed in the focal plane of the lens L.

We are interested in spatial correlations which can be observed in the far field, where the particle-like character of the radiation field (photon pairs) is displayed. The optical setup which can be used is described schematically in Figure 1. The plane-wave pump field propagates along the z-axis, which we take as the system axis, and is normally incident from the left onto a $\chi^{(2)}$ crystal slab of length l_c. Intensity and correlation measurements of the fluorescence far-field are performed in the focal plane of the lens L, which performs the Fourier transform of the down-converted field from the output face of the crystal. The main reason for introducing of the pupil P on the output face of the crystal is elimination of divergencies which arise in a system of infinite transverse size [16]; this pupil also fixes the spatial resolution of the system.

Focusing on the down-converted field emitted close to the degenerate frequency, we consider a single quasi-monochromatic wave of carrier frequency ω_s. Let us denote with $A(z,\mathbf{x},t)$ the corresponding complex amplitude envelope operator, t indicates time and $\mathbf{x}=(x,y)$ the coordinate vector in the plane orthogonal to z-axis. We shall denote by a small a its Fourier transform with respect to

the time and the transverse coordinates (x, y), that is

$$a(z, \mathbf{q}, \Omega) = \int \frac{\mathrm{d}t}{\sqrt{2\pi}} \int \frac{\mathrm{d}\mathbf{x}}{2\pi} A(z, \mathbf{x}, t) \mathrm{e}^{-\mathrm{i}\mathbf{q}\cdot\mathbf{x}+\mathrm{i}\Omega t} \, .$$

On the other hand no special notation is introduced for the transform with respect to time only, $A(z, \mathbf{x}, \Omega)$, since this should not lead to misunderstanding. In the linear regime, assuming that pump depletion and losses are negligible, the propagation equations take the form [17,19]

$$\frac{\mathrm{d}}{\mathrm{d}z} a(z, \mathbf{q}, \Omega) = -\mathrm{i}(k_z(\mathbf{q}, \Omega) - k_\mathrm{s}) a(z, \mathbf{q}, \Omega) + \sigma \mathrm{e}^{-\mathrm{i}\Delta_0 z} a^\dagger(z, -\mathbf{q}, -\Omega), \tag{1a}$$

$$\frac{\mathrm{d}}{\mathrm{d}z} a^\dagger(z, -\mathbf{q}, -\Omega) = \mathrm{i}(k_z(-\mathbf{q}, -\Omega) - k_\mathrm{s}) a^\dagger(z, -\mathbf{q}, -\Omega) + \sigma^* \mathrm{e}^{\mathrm{i}\Delta_0 z} a(z, \mathbf{q}, \Omega). \tag{1b}$$

They are written here in the paraxial and slowly-varying envelope approximations. The first term on the r.h.s. describes linear propagation inside the crystal; $k_z(\mathbf{q}, \Omega)$ is the wave vector component along the z-axis of the wave with the frequency $\omega_\mathrm{s} + \Omega$ and the transverse wave vector $\mathbf{q}$. This component has the following quadratic expansion

$$k_z(\mathbf{q}, \Omega) \equiv \sqrt{k^2(\omega_\mathrm{s} + \Omega) - q^2} \simeq k_\mathrm{s} + k'_\mathrm{s}\Omega + \frac{1}{2} k''_\mathrm{s} \Omega^2 - \frac{q^2}{2k_\mathrm{s}}, \tag{2}$$

where we used the notation $k_\mathrm{s} \equiv k(\omega_\mathrm{s})$, and $k'_\mathrm{s} \equiv (\mathrm{d}k/\mathrm{d}\omega)_{\omega=\omega_\mathrm{s}}$. The second term in equations (1) describes the nonlinear interaction between different modes; the coupling constant σ is proportional to the pump field amplitude and to the nonlinear susceptibility. Only pairs of modes with opposite transverse wave vectors, $\mathbf{q}$ and $-\mathbf{q}$, and with frequencies $\omega_\mathrm{s} + \Omega$ and $\omega_\mathrm{s} - \Omega$ are coupled as a consequence of conservation of the energy and the transverse momentum.

By solving equations (1), we can write explicitly the input-output transformation which relates the field operators in the output face of the crystal (plane $z = l_\mathrm{c}$) to those in the input face (plane $z = 0$); we obtain (see *e.g.* [19])

$$a(l_\mathrm{c}, \mathbf{q}, \Omega) = U(\mathbf{q}, \Omega) a(0, \mathbf{q}, \Omega) + V(\mathbf{q}, \Omega) a^\dagger(0, -\mathbf{q}, -\Omega), \tag{3}$$

where the coefficients $U(\mathbf{q}, \Omega)$ and $V(\mathbf{q}, \Omega)$ are given by

$$U(\mathbf{q}, \Omega) = \exp\left[\mathrm{i}\left(k_z(\mathbf{q}, \Omega) - k_\mathrm{s} - \frac{\Delta(\mathbf{q}, \Omega)}{2}\right) l_\mathrm{c}\right] \times \left[\cosh(\Gamma(\mathbf{q}, \Omega) l_\mathrm{c}) + \mathrm{i}\frac{\Delta(\mathbf{q}, \Omega)}{2\Gamma(\mathbf{q}, \Omega)} \sinh(\Gamma(\mathbf{q}, \Omega) l_\mathrm{c})\right], \tag{4a}$$

$$V(\mathbf{q}, \Omega) = \exp\left[\mathrm{i}\left(k_z(\mathbf{q}, \Omega) - k_\mathrm{s} - \frac{\Delta(\mathbf{q}, \Omega)}{2}\right) l_\mathrm{c}\right] \times \frac{\sigma}{\Gamma(\mathbf{q}, \Omega)} \sinh(\Gamma(\mathbf{q}, \Omega) l_\mathrm{c}), \tag{4b}$$

with

$$\Gamma(\mathbf{q}, \Omega) = \sqrt{|\sigma|^2 - \frac{\Delta(\mathbf{q}, \Omega)^2}{4}}, \tag{5a}$$

$$\Delta(\mathbf{q}, \Omega) = k_z(\mathbf{q}, \Omega) + k_z(-\mathbf{q}, -\Omega) - k_\mathrm{p}. \tag{5b}$$

We shall consider situations where the parametric gain is not negligible, that is $|\sigma| l_\mathrm{c}$ is at least on the order of unity, although spontaneous fluorescence can be observed even for small values of this parameter (see *e.g.* [22], Chap. 17). From the expression of $\Gamma(\mathbf{q}, \Omega)$, we see that the most efficient down-conversion occurs in the modes for which $\Delta(\mathbf{q}, \Omega) < 2|\sigma|$; $\Delta(\mathbf{q}, \Omega) l_\mathrm{c}$ is the corresponding phase-mismatch accumulated during propagation and depends on the linear dispersion properties of the medium. Using equation (2), it can be written in the form

$$\Delta(\mathbf{q}, \Omega) l_\mathrm{c} \simeq \Delta_0 l_\mathrm{c} - \left(\frac{q^2}{q_0^2} - \mathrm{sign}(k''_\mathrm{s}) \frac{\Omega^2}{\Omega_0^2}\right), \tag{6}$$

where

$$q_0 = \sqrt{\frac{k_\mathrm{s}}{l_\mathrm{c}}}, \quad \Omega_0 = \sqrt{\frac{1}{|k''_\mathrm{s}| l_\mathrm{c}}}, \tag{7}$$

give the amplification bandwidths in the spatial frequency domain and in the time frequency domain, respectively, and

$$\Delta_0 = 2k_\mathrm{s} - k_\mathrm{p}, \tag{8}$$

is the collinear phase-mismatch at the degenerate frequency.

We shall be interested in the situation where Δ_0 takes a small positive value. In this case the waves of frequency $\sim \omega_\mathrm{s}$ that are best phase-matched are those with a transverse wave vector component close to

$$q_\mathrm{m} = \sqrt{k_\mathrm{s}^2 - (k_\mathrm{p}/2)^2} \simeq \sqrt{k_\mathrm{s} \Delta_0}. \tag{9}$$

Thus, around the frequency ω_s we have a radiation cone with a half-aperture angle equal to $\sim q_\mathrm{m}/k_\mathrm{s}$. This angle shrinks to zero when $\Delta_0 \to 0$, that can be obtained *e.g.* by rotating the crystal around the optical axis. When observed in the far field, the cross-section of this cone gives a characteristic ring pattern (see *e.g.* [17,18]).

In our analysis we shall use the following unitarity conditions:

$$|U(\mathbf{q}, \Omega)|^2 - |V(\mathbf{q}, \Omega)|^2 = 1, \quad U(\mathbf{q}, \Omega) V(-\mathbf{q}, -\Omega) = U(-\mathbf{q}, -\Omega) V(\mathbf{q}, \Omega), \tag{10}$$

which guarantee the conservation of the free-field commutation relations

$$\left[a(z, \mathbf{q}, \Omega), a^\dagger(z, \mathbf{q}', \Omega')\right] = \delta(\mathbf{q} - \mathbf{q}')\delta(\Omega - \Omega') \quad [a(z, \mathbf{q}, \Omega), a(z, \mathbf{q}', \Omega')] = 0. \tag{11}$$

The field in the detection plane $z = l_c + 2f$ is related to the field in the output plane of the crystal $z = l_c$ through the transformation:

$$A(l_c + 2f, \mathbf{x}, t) = \frac{-\mathrm{i}}{\lambda_s f} \int \mathrm{d}\mathbf{x}' Q(\mathbf{x}') A(l_c, \mathbf{x}', t) \mathrm{e}^{-\mathrm{i}\frac{2\pi}{\lambda_s f}\mathbf{x}\cdot\mathbf{x}'} + \frac{-\mathrm{i}}{\lambda_s f} \int \mathrm{d}\mathbf{x}' (1 - Q(\mathbf{x}')) C(\mathbf{x}', t) \mathrm{e}^{-\mathrm{i}\frac{2\pi}{\lambda_s f}\mathbf{x}\cdot\mathbf{x}'}. \quad (12)$$

where $Q(\mathbf{x})$ is the pupil frame function, equal to unity within the pupil area S_p, and zero elsewhere; $\lambda_s = 2\pi/k_s$. The first term in equation (12) corresponds to the classical Fresnel transformation from the pupil to the focal plane of the lens. The field operator $C(\mathbf{x}, t)$ in the second term obeys the free-field commutation relations identical to (11), is independent of $A(\mathbf{x}, t)$ and its quantum state is vacuum. As underlined in [16], the quantum theory requires this term which gives the contribution from the vacuum fluctuations coming from the pupil screen outside the pupil. This term ensures that $A(l + 2f, \mathbf{x}, t)$ satisfies the free-field commutation relations. Its role is analogous to that of an operator used to describe the vacuum fluctuations entering an unused port of a beam splitter. However, in the following we shall omit it, since it does not give any contribution in the calculation of the it normally ordered correlation functions in the detection plane. By combining equations (3, 12), one obtains the desired input-output transformation between the field operator in the input plane of the crystal $A_{in}(\mathbf{x}, t) \equiv A(0, \mathbf{x}, t)$ and that in the detection plane $A_{out}(\mathbf{x}, t) \equiv A(l_c + 2f, \mathbf{x}, t)$:

$$\begin{aligned} A_{out}(\mathbf{x}, \Omega) &= \frac{-\mathrm{i}}{\lambda_s f} \int \frac{\mathrm{d}\mathbf{q}}{2\pi} \int_{S_p} \mathrm{d}\mathbf{x}' \, \mathrm{e}^{\mathrm{i}\left[\mathbf{q} - \frac{2\pi}{\lambda_s f}\mathbf{x}\right]\cdot\mathbf{x}'} \\ &\quad \times \left[U(\mathbf{q}, \Omega) a_{in}(\mathbf{q}, \Omega) + V(\mathbf{q}, \Omega) a_{in}^\dagger(-\mathbf{q}, -\Omega)\right] \\ &= \frac{2\pi\mathrm{i}}{\lambda_s f} \int \mathrm{d}\mathbf{x}' p(\mathbf{x} - \mathbf{x}') \left[\tilde{U}(\mathbf{x}', \Omega) a_{in}\left(\frac{2\pi}{\lambda_s f}\mathbf{x}', \Omega\right) \right. \\ &\quad \left. + \tilde{V}(\mathbf{x}', \Omega) a_{in}^\dagger\left(-\frac{2\pi}{\lambda_s f}\mathbf{x}', -\Omega\right)\right], \end{aligned} \quad (13)$$

where we have introduced the functions $\tilde{U}(\mathbf{x}, \Omega)$ and $\tilde{V}(\mathbf{x}, \Omega)$ defined in the coordinate space

$$\begin{aligned} \tilde{U}(\mathbf{x}, \Omega) &= U\left(\frac{2\pi}{\lambda_s f}\mathbf{x}, \Omega\right), \\ \tilde{V}(\mathbf{x}, \Omega) &= V\left(\frac{2\pi}{\lambda_s f}\mathbf{x}, \Omega\right), \end{aligned} \quad (14)$$

which vary on a scale on the order of

$$x_0 = \frac{\lambda_s f}{2\pi} q_0, \quad (15)$$

while

$$p(\mathbf{x}) = \left(\frac{-\mathrm{i}}{\lambda_s f}\right)^2 \int_{S_p} \mathrm{d}\mathbf{x}' \mathrm{e}^{\mathrm{i}\frac{2\pi}{\lambda_s f}\mathbf{x}'\cdot\mathbf{x}}, \quad (16)$$

is the diffraction pattern of the pupil in the far-field plane. It varies on the scale $x_{diff} = \lambda_s f/\sqrt{S_p}$, the size of the diffraction spot in the detection plane. Assuming that the pupil is symmetric with respect to the optical axis, $p(\mathbf{x})$ is an even real function centered on the origin and with the typical scale of the area $S_{diff} = (\lambda_s f)^2/S_p$. For example, for a square aperture of side a centered in the origin, one has

$$p(\mathbf{x}) = -\left(\frac{a}{\lambda_s f}\right)^2 \mathrm{sinc}\left(\frac{\pi a}{\lambda_s f} x\right) \mathrm{sinc}\left(\frac{\pi a}{\lambda_s f} y\right). \quad (17)$$

We also mention the case of a circular aperture of radius a, for which

$$p(\mathbf{x}) = -2\pi \left(\frac{a}{\lambda_s f}\right)^2 \frac{J_1\left(\frac{2\pi a}{\lambda_s f}|\mathbf{x}|\right)}{\frac{2\pi a}{\lambda_s f}|\mathbf{x}|}, \quad (18)$$

where J_1 is the Bessel function of the first kind of order one.

3 Far-field fluorescence pattern

Since we are interested in the spontaneous parametric down-conversion, we assume the input field to be in the vacuum state. The average intensity distribution on the detection plane is proportional to the mean value of the photon flux density operator

$$I(\mathbf{x}, t) = A_{out}^\dagger(\mathbf{x}, t) A_{out}(\mathbf{x}, t), \quad (19)$$

which gives the mean number of photons crossing the detection plane in point $\mathbf{x}$ per unit area and unit time. Using equations (13, 11), we obtain

$$\langle I(\mathbf{x}, t)\rangle = \int \frac{\mathrm{d}\Omega}{2\pi} \int \mathrm{d}\mathbf{x}' |p(\mathbf{x}' - \mathbf{x})|^2 |\tilde{V}(\mathbf{x}', \Omega)|^2. \quad (20)$$

Let us now assume that the pupil is large enough so that the far-field diffraction spread x_{diff} is small compared to the typical scale x_0 of the functions $\tilde{U}$ and $\tilde{V}$, that is

$$\alpha = \frac{x_0}{x_{diff}} \gg 1. \quad (21)$$

Then, integrating over an area large compared to S_{diff} we can use the following approximations:

$$\begin{aligned} p(\mathbf{x}) &\approx -\delta(\mathbf{x}) \, , \\ |p(\mathbf{x})|^2 &\approx \frac{1}{S_{diff}} \delta(\mathbf{x}), \end{aligned} \quad (22)$$

and equation (20) reduces to

$$\langle I(\mathbf{x}, t)\rangle = \frac{1}{S_{diff}} \int \frac{\mathrm{d}\Omega}{2\pi} |\tilde{V}(\mathbf{x}, \Omega)|^2. \quad (23)$$

As we shall see in the next section, in this small-diffraction limit analytical calculations are greatly simplified. Moreover, only in this limit spatial intensity correlation effects can be observed, since a small pupil would eliminate the separation of the emitted twin photons in the far field by

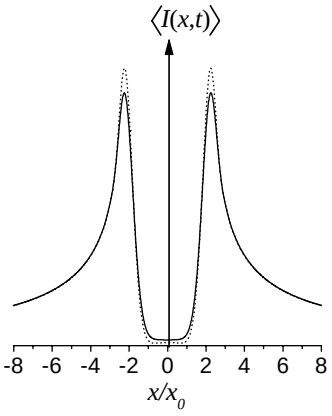

Fig. 2. 1-D case. Average intensity distribution in the detection plane for $\alpha = 3$. The other parameters are $\Delta_0 l_c = 8$ and $|\sigma l_c| = 2.0$. The dashed line, corresponding to the $\alpha \gg 1$ approximation (23), is close to the exact solution (20) (full line).

introducing a too large diffraction spread. On the other hand, it is important to keep the size of the pupil area finite since $\langle I(\mathbf{x},t)\rangle$ diverges for $S_p \to \infty$, as follows from equation (23). This should be expected in a system of infinite transverse dimensions.

We have investigated numerically the approximation (23) for large finite values of α. For the sake of simplicity numerical calculations were performed for a 1-D version of the model, where the aperture is a one-dimensional slit of width a. Figure 2 shows the corresponding intensity profile calculated numerically using equation (20) (solid line) and equation (23) (dashed line), for $\alpha = 3$ and $\Delta_0 l_c = 8$. As seen from this figure, the approximation (23) is quite good even for moderate values of α. The two intensity peaks correspond to the waves that are best phase-matched, *i.e.* with $q \simeq q_m$ at $\Omega \simeq 0$. Using equation (15) which relates the spatial scales with the scales in the spatial frequency space, we can evaluate the distance x_m of these maxima from the optical axis as $x_m/x_0 = \sqrt{\Delta_0 l_c}$. In Figure 2 we have $x_m/x_0 = 2.8$. In 2-D we expect a similar behavior, with the 2-D figures similar to the corresponding 1-D rotated around the z-axis: notice that *e.g.* for the limiting expression (23) the intensity distribution in 2-D is obtained by rotating the 1-D profile around the optical axis. This leads to a ring pattern similar to the one observed in the experiment of Lantz and Devaux with a lithium triborate crystal (LBO) cut for the type-I phase matching [18].

4 Quantum correlations in the far-field fluorescence pattern

Quantum correlations in the intensity fluctuations are described by the normally ordered correlation function

$$\begin{aligned} G(\mathbf{x},t;\mathbf{x}',t') &= \langle : \delta I(\mathbf{x},t)\delta I(\mathbf{x}',t') : \rangle \\ &= \langle A^\dagger_{\rm out}(\mathbf{x},t)A^\dagger_{\rm out}(\mathbf{x}',t')A_{\rm out}(\mathbf{x}',t')A_{\rm out}(\mathbf{x},t)\rangle \\ &\quad - \langle A^\dagger_{\rm out}(\mathbf{x},t)A_{\rm out}(\mathbf{x},t)\rangle\langle A^\dagger_{\rm out}(\mathbf{x}',t')A_{\rm out}(\mathbf{x}',t')\rangle, \end{aligned} \quad (24)$$

where $\delta I(\mathbf{x},t) = I(\mathbf{x},t) - \langle I(\mathbf{x},t)\rangle$ and : : denotes normal ordering. The Gaussian character of the fluctuations allows us to express the higher-order correlation functions of the field operators through the second-order correlation functions $\langle A^\dagger_{\rm out}(\mathbf{x},t)A_{\rm out}(\mathbf{x}',t')\rangle$ and $\langle A_{\rm out}(\mathbf{x},t)A_{\rm out}(\mathbf{x}',t')\rangle$. In particular, for the correlation function $G(\mathbf{x},t;\mathbf{x}',t')$ we find

$$\begin{aligned} G(\mathbf{x},t;\mathbf{x}',t') &= |\langle : A^\dagger_{\rm out}(\mathbf{x},t)A_{\rm out}(\mathbf{x}',t') : \rangle|^2 \\ &\quad + |\langle : A_{\rm out}(\mathbf{x},t)A_{\rm out}(\mathbf{x}',t') : \rangle|^2. \end{aligned} \quad (25)$$

Below we shall investigate the Fourier transform in time of this correlation function

$$\tilde G(\mathbf{x},\mathbf{x}';\Omega) = \int \mathrm{d}t\ \mathrm{e}^{-\mathrm{i}\Omega t}\langle : \delta I(\mathbf{x},t)\delta I(\mathbf{x}',0) : \rangle. \quad (26)$$

The latter function can be evaluated using the input-output transformation (13) and the commutation relation (11); we find

$$\tilde G(\mathbf{x},\mathbf{x}';\Omega) = \sum_{i=1,2}\int \mathrm{d}\Omega'\ \Gamma_i(\mathbf{x},\mathbf{x}';\Omega+\Omega')\Gamma_i^*(\mathbf{x},\mathbf{x}';\Omega'), \quad (27)$$

where

$$\begin{aligned} \Gamma_1(\mathbf{x},\mathbf{x}';\Omega) &= \int \mathrm{d}t\ \mathrm{e}^{-\mathrm{i}\Omega t}\langle A^\dagger_{\rm out}(\mathbf{x},t)A_{\rm out}(\mathbf{x}',0)\rangle \quad (28a)\\ &= \int \mathrm{d}\mathbf{x}''\, p^*(\mathbf{x}''-\mathbf{x})p(\mathbf{x}''-\mathbf{x}')|\tilde V(\mathbf{x}'',\Omega)|^2, \\ \Gamma_2(\mathbf{x},\mathbf{x}';\Omega) &= \int \mathrm{d}t\ \mathrm{e}^{-\mathrm{i}\Omega t}\langle A_{\rm out}(\mathbf{x},t)A_{\rm out}(\mathbf{x}',0)\rangle \quad (28b)\\ &= \int \mathrm{d}\mathbf{x}''\ p(\mathbf{x}''-\mathbf{x})p(\mathbf{x}''+\mathbf{x}') \\ &\quad \times \tilde U(\mathbf{x}'',\Omega)\tilde V(-\mathbf{x}'',-\Omega), \end{aligned}$$

are the temporal Fourier transforms of the field correlation functions.

Figure 3 shows the calculated intensity correlation function $\tilde G(x,x';0)$ in the one-dimensional case, for a fixed value of x', $x'/x_0 = 2$, and for different values the parameter $\alpha = x_0/x_{\rm diff}$. Two peaks are clearly distinguishable as long as $\alpha > 1$, their widths $\sim x_{\rm diff}$ being much smaller than x_0. The first peak at $x = x'$ arises from self-correlations, while the second, at $x = -x'$, indicates the existence of cross-correlations between symmetrical regions in the transverse plane.

Note that in Figure 3 the self- and cross-correlation peaks are shifted farther apart from the optical axis as compared to the maxima of the mean intensity. The explanation is in our choice of parameters for this figure which are $x_m/x_0 = 1.4$ and $x'/x_0 = 2$. It is important to underline that these correlations peaks exist for arbitrary position of the point x' close to the maxima of intensity x_m within the distance x_0 determined by the phase-matching within the crystal.

Such a kind of spatial quantum correlation have already been investigated in the context of a multimodal analysis for an optical parametric oscillator below threshold [9]. These correlations have their origin in the twin photon emission processes occurring in the nonlinear

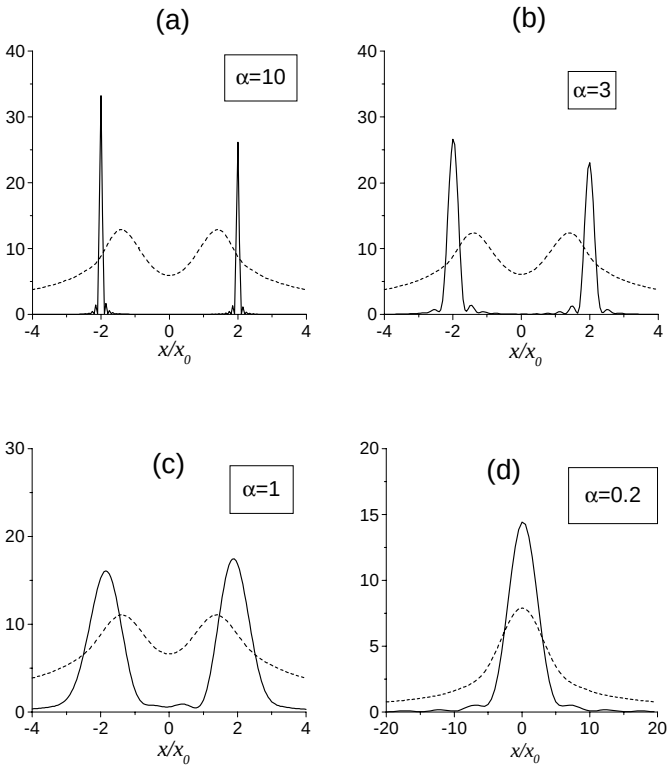

Fig. 3. $\tilde{G}(x,x';0)$ is plotted as a function of x for different values of α, keeping $x'/x_0 = 2$ (full line); $\Delta_0 l_c = 2$ and $|\sigma l_c| = 1.5$. The peak for $x = -x'$ is higher than the peak for $x = x'$ as long as $\alpha > 1$, while it disappears for $\alpha < 1$. The dashed line is the corresponding intensity profile.

crystal, according to the energy and momentum conservation laws. The normally ordered correlation function $G(\mathbf{x},t;\mathbf{x}',t')$ is indeed related to the joint probability density $W(\mathbf{x},t;\mathbf{x}',t')$ of detecting a photon in point $\mathbf{x}$ at time t, and another photon at $\mathbf{x}'$ at time t'; precisely we have [20]

$$W(\mathbf{x},t;\mathbf{x}',t') \propto \langle : I_{\rm out}(\mathbf{x},t) I_{\rm out}(\mathbf{x}',t') : \rangle = \langle I_{\rm out}(\mathbf{x},t)\rangle \langle I_{\rm out}(\mathbf{x}',t')\rangle + G(\mathbf{x},t;\mathbf{x}',t'). \quad (29)$$

Close to degeneracy, the twin photons of each down-converted pair are emitted symmetrically with respect to the system axis, because of momentum conservation in the transverse plane. They can therefore be resolved separately in the two symmetrical points $\mathbf{x} = \pm(\lambda f/2\pi)\mathbf{q}$ of the detection plane, $\pm\mathbf{q}$ being their opposite transverse wave vectors. The high correlation peak exhibited by the intensity correlation function for $\mathbf{x}' = -\mathbf{x}$ is therefore a clear spatial evidence of the emission of correlated photon pairs. Moreover, we see from Figures 3a and 3b that the cross-correlation peak can be higher than the self-correlation peak, *i.e.*

$$\tilde{G}(\mathbf{x},-\mathbf{x};0) > \tilde{G}(\mathbf{x},\mathbf{x};0). \quad (30)$$

Now we shall demonstrate that this phenomenon cannot take place for a classical field since it implies a violation of the Cauchy-Schwartz inequality. The adjective *classical* refers here to such fields that possess a non-negative Glauber P-representation.

Let us consider the fluctuations of the number of photons per unit area collected in a finite time interval $[-T_{\rm d}/2, T_{\rm d}/2]$:

$$\delta N(\mathbf{x}) = \int_{-T_{\rm d}/2}^{T_{\rm d}/2} {\rm d}t\ \delta I_{\rm out}(\mathbf{x},t). \quad (31)$$

If the P-representation exists, it can be used in order to express the mean value of the normally ordered product of $\delta N(\mathbf{x})$ and $\delta N(\mathbf{x}')$ in the form

$$\langle : \delta N(\mathbf{x}) \delta N(\mathbf{x}') : \rangle = \langle \delta N(\mathbf{x}) \delta N(\mathbf{x})' \rangle_P, \quad (32)$$

where $\langle \cdots \rangle_P$ denotes the classical-looking average over the P-functional of the field [20]. For a classical field P is non-negative and has all the properties of a probability distribution. The r.h.s. of equation (32) is therefore an inner product and the Cauchy-Schwartz inequality imposes that

$$|\langle \delta N(\mathbf{x}) \delta N(\mathbf{x}') \rangle_P|^2 \leq \langle \delta N(\mathbf{x})^2 \rangle_P \langle \delta N(\mathbf{x}')^2 \rangle_P\ . \quad (33)$$

On the other hand, taking $T_{\rm d} \gg \Omega_0^{-1}$, we have under stationarity conditions

$$\begin{aligned} \langle : \delta N(\mathbf{x}) \delta N(\mathbf{x}') : \rangle &= \int_{-T_{\rm d}/2}^{T_{\rm d}/2} {\rm d}t \int_{-T_{\rm d}/2}^{T_{\rm d}/2} {\rm d}t' \langle : \delta I(\mathbf{x},t) \delta I(\mathbf{x}',t') : \rangle \\ &\simeq T_{\rm d} \int_{-\infty}^{\infty} {\rm d}\tau \langle : \delta I(\mathbf{x},\tau) \delta I(\mathbf{x}',0) : \rangle \\ &= T_{\rm d} \tilde{G}(\mathbf{x},\mathbf{x}';0). \end{aligned} \quad (34)$$

Therefore, relation (33) can be written as

$$\tilde{G}(\mathbf{x},\mathbf{x}';0)^2 \leq \tilde{G}(\mathbf{x},\mathbf{x};0)\ \tilde{G}(\mathbf{x}',\mathbf{x}';0). \quad (35)$$

Noting that for symmetry reasons $\tilde{G}(-\mathbf{x},-\mathbf{x};0) = \tilde{G}(\mathbf{x},\mathbf{x};0)$, we see that relation (30) implies a violation of this inequality in the special case with $\mathbf{x}' = -\mathbf{x}$.

We shall see in the next section that this non-classical behavior of the correlation function can lead to the shot-noise reduction for the fluctuations of the photocurrent difference.

5 Shot-noise reduction in the photocurrent difference

Let us now consider two identical detectors, 1 and 2, which intercept photons crossing two arbitrary symmetrical regions R_1 and R_2 with the area $S_{\rm d}$ in the detection plane, as shown schematically in Figure 4. The corresponding photocurrent operators $i_1(t)$ and $i_2(t)$ under stationary conditions have the equal constant mean values:

$$\langle i_1(t) \rangle = \langle i_2(t) \rangle = \eta \int_{R_1} {\rm d}\mathbf{x} \langle I(\mathbf{x},t) \rangle, \quad (36)$$

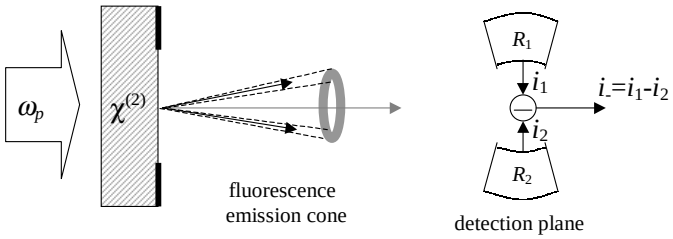

Fig. 4. Detection scheme for intensity squeezing measurements in the OPA far field. The photocurrents generated on the detection region R_1 and R_2 are electronically subtracted, giving $i_- = i_1 - i_2$.

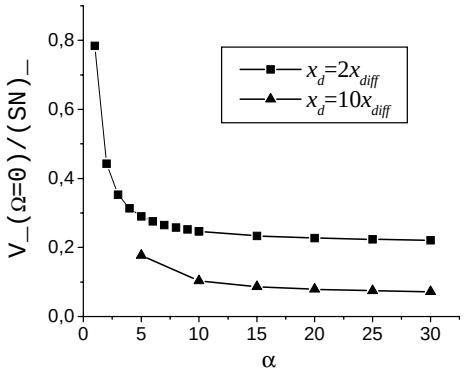

Fig. 5. Numerical calculation of the amount of noise reduction as a function of α, for two fixed values of the ratio $x_{\rm d}/x_{\rm diff}$.

where η denotes the quantum efficiency of detectors and the mean intensity distribution $\langle I(\mathbf{x},t)\rangle$ is given by equation (20).

We expect the quantum fluctuations in the photocurrent difference $i_-(t) = i_1(t) - i_2(t)$ to be reduced below the shot noise as a consequence of emission of the correlated photon pairs. In fact the photocurrents i_1 and i_2 play a role similar to the photocurrents obtained from detection of the signal and idler beams in the optical parametric oscillator [21]. In the latter case the photocurrent difference between the twin signal and idler beams exhibits fluctuations below the shot-noise level. Similarly in our case reduction of the fluctuations in i_- below the shot-noise level is the consequence of spatial entanglement between the signal and idler field in the regions R_1 and R_2. The noise spectrum $V_-(\Omega)$ of the photocurrent difference can be expressed in terms of the intensity correlation function $\tilde{G}(\mathbf{x},\mathbf{x}';\Omega)$ as:

$$V_-(\Omega) = (SN)_- + S_-(\Omega), \tag{37a}$$

$$\begin{aligned} S_-(\Omega) &= \int \mathrm{d}t\, \mathrm{e}^{-\mathrm{i}\Omega t} \langle : \delta i_-(t)\delta i_-(0) : \rangle \\ &= 2\langle S_{11}(\Omega) - S_{12}(\Omega)\rangle \\ &= 2\eta^2 \int_{R_1} \mathrm{d}\mathbf{x} \int_{R_1} \mathrm{d}\mathbf{x}' (\tilde{G}(\mathbf{x},\mathbf{x}';\Omega) - \tilde{G}(\mathbf{x},-\mathbf{x}';\Omega)). \end{aligned} \tag{37b}$$

In this expression, we have separated explicitly the shot-noise contribution $(SN)_- = \langle i_1\rangle + \langle i_2\rangle$ from the normally ordered component of the spectra

$$\begin{aligned} S_{jl}(\Omega) &= \int \mathrm{d}t\ \mathrm{e}^{-\mathrm{i}\Omega t} \langle : \delta i_j(t)\delta i_l(0) : \rangle \\ &= \eta^2 \int_{R_j} \mathrm{d}\mathbf{x} \int_{R_l} \mathrm{d}\mathbf{x}'\ \tilde{G}(\mathbf{x},\mathbf{x}';\Omega), \qquad (j,l=1,2), \end{aligned} \tag{38}$$

that describe the photocurrent cross-correlations between the regions 1 and 2 (for $j \neq l$) and self-correlations (for $j = l$). A significant noise reduction can be observed provided the detection area $S_{\rm d}$ is at least of the order of $S_{\rm diff}$, $S_{\rm d} \gtrsim S_{\rm diff}$ and simultaneously the small-diffraction condition (21) is fulfilled, that is $\alpha \gg 1$. Indeed, under the latter condition the inequality (30) is satisfied and, as a consequence, $S_-(\Omega)$ takes negatives values as can be inferred from equation (37b) (this occurs in fact within a frequency band of width Ω_0 around $\Omega = 0$). The photocurrent difference i_- displays therefore noise reduction below the shot-noise level $(SN)_-$.

Taking $S_{\rm d} \gtrsim S_{\rm diff}$, and using the fact that the functions (14) are nearly uniform in the regions of area $S_{\rm diff}$, where the diffraction pattern function (16) is not negligible, we can apply the same approximation that led us to equation (23) (see Eq. (22)). In this manner we obtain the following expression for the normally ordered component of the spectrum

$$\begin{aligned} S_-(\Omega) \simeq 2\eta^2 \frac{1}{S_{\rm diff}} \int_{R_1} \mathrm{d}\mathbf{x} \int \frac{\mathrm{d}\Omega'}{2\pi} \Big[&|\tilde{V}(\mathbf{x},\Omega+\Omega')|^2 |\tilde{V}(\mathbf{x},\Omega')|^2 \\ &- \tilde{U}(\mathbf{x},\Omega+\Omega')\tilde{V}(\mathbf{x},\Omega+\Omega')\tilde{U}^*(\mathbf{x},\Omega')\tilde{V}^*(\mathbf{x},\Omega') \Big]. \end{aligned} \tag{39}$$

Within the same approximation the shot noise is given by

$$(SN)_- = 2\langle i_1\rangle \simeq 2\eta \frac{1}{S_{\rm diff}} \int_{R_1} \mathrm{d}\mathbf{x} \int \frac{\mathrm{d}\Omega}{2\pi} |\tilde{V}(\mathbf{x},\Omega)|^2. \tag{40}$$

According to unitarity condition (10), for $\Omega = 0$ the integrand of equation (39) reduces to $-|\tilde{V}(\mathbf{x},\Omega)|^2$. From definitions (37b, 40) we obtain

$$V_-(0) \simeq (1-\eta)(SN)_-. \tag{41}$$

Noise reduction at zero frequency is therefore complete in the case of ideal detection ($\eta = 1$), provided that $\alpha \gg 1$ and $S_{\rm d} \gtrsim S_{\rm diff}$.

Numerical calculation of the amount of noise reduction in the photocurrent difference with respect to the shot noise have been performed in the one-dimensional case in order to verify our analytical result. Figure 5 shows the zero-frequency value of the spectrum of i_- normalized to the shot noise as a function of α for two values of the ratio $x_{\rm d}/x_{\rm diff}$, $x_{\rm d}$ being the linear size of the detection regions. Two symmetrical detectors have been taken centered at the maxima of the mean intensity, $x_{\rm m} = \pm x_0\sqrt{\Delta_0 l_{\rm c}}$. Note that if we assume x_0 to be fixed by the crystal characteristics and the geometry of the experiment then increasing

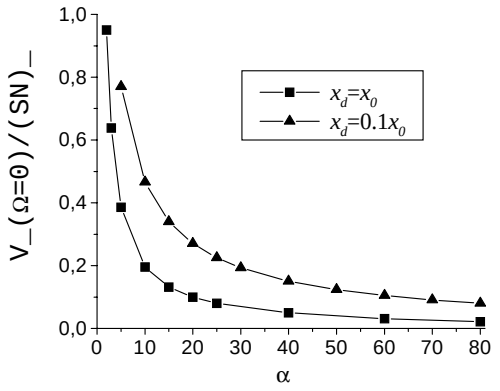

Fig. 6. Same plot as in previous figure, but the detection area is kept fixed.

α amounts to enlarging the pupil size, and thus $x_{\rm diff}$ decreases along the horizontal α-axis. Since each line in Figure 5 corresponds to a fixed ratio of the detector size $x_{\rm d}$ to the diffraction spread $x_{\rm diff}$, the detector size also decreases for increasing values of α. This explains why in this figure perfect noise reduction $V_-(0) = 0$ is not achieved for $\alpha \to \infty$.

Figure 6 represents the same quantity as Figure 5, but for $x_{\rm d}$ fixed. We see that $V_-(0)/(SN)_-$ goes to zero for increasing values of α even when the two detection areas cover only a small fraction of the light beam, $x_{\rm d} = 0.1x_0$, in agreement with our analytical result (41).

Finally we note that the fluctuations of the number of photoelectrons for a single detector are given by:

$$\langle(\delta N_1(t))^2\rangle = \langle(\delta N_2(t))^2\rangle \simeq T_{\rm d}(SN)_1 + \eta^2 T_{\rm d}\frac{1}{S_{\rm diff}}\int_{R_1}{\rm d}\mathbf{x}\int\frac{{\rm d}\Omega}{2\pi}|\tilde{V}(\mathbf{x},\Omega)|^4. \quad (42)$$

For large amplification the second term is very large compared to the shot noise. Therefore, the photon statistics of individual beams crossing detectors 1 and 2 are super-Poissonian and are similar to the statistics of thermal light. However, equation (41) shows that these fluctuations are highly correlated. According to this result, intensity fluctuations in region 1 and 2 are quite substantial, but very well synchronized.

6 Conclusions

We have analyzed the spatial aspects of quantum entanglement created in the far field of the light emitted in spontaneous parametric down-conversion in a cavityless traveling-wave configuration. The main results are that

(1) the normally ordered spatial correlation function $\tilde{G}(\mathbf{x},\mathbf{x}';\Omega)$ displays two peaks centered, respectively, at $\mathbf{x}' = \mathbf{x}$ (self-correlation) and $\mathbf{x}' = -\mathbf{x}$ (cross-correlation). In the small-diffraction limit, $\alpha \gg 1$ the cross-correlation peak is higher than the self-correlation peak. This proves the quantum nature of the spatial fluctuations in the down-converted field;

(2) the intensity fluctuations in two arbitrary symmetrical regions of the far field are very well synchronized. Precisely, the fluctuations in the intensity difference are largely below the shot-noise level.

Even if such results are similar to those of [9], the essential advantage of the present analysis with respect to that carried out in the case of the optical parametric oscillator below threshold lies in the fact that the final expressions are substantially simpler. Especially, it was possible to prove analytically that the suppression of quantum fluctuations in the intensity difference is complete for zero frequency in the limit of low diffraction and ideal quantum efficiency. No such a clear and strong result is possible in the case of optical parametric oscillators, in which one can show numerically only that the reduction below shot noise can become quite substantial, but it seems impossible to prove that the noise suppression can become complete by moving appropriately in the parameter space of the system. In Appendix A we establish the connection between the parameters of the cavityless case and that of the optical parametric oscillators, which plays a crucial role in the determination of the effects shown in this paper.

Appendix A

As we have seen in Section 5, the quantum noise reduction in V_- increases when the parameter α is increased. In the case of the Optical Parametric Oscillator (OPO) below threshold [9] the same happens when an appropriate parameter ζ is decreased. In this appendix we want to show the connection between the two parameters. First of all, from equation (21) and the definitions

$$x_{\rm diff} = \frac{\lambda_{\rm s} f}{\sqrt{S_{\rm p}}}, \quad x_0 = \frac{\lambda_{\rm s} f}{2\pi} q_0, \quad q_0 = \sqrt{\frac{k_{\rm s}}{l_{\rm c}}} \quad (A.1)$$

we obtain the expression

$$\alpha = \left(\frac{S_{\rm p}}{2\pi\lambda l_{\rm c}}\right)^{1/2}. \quad (A.2)$$

On the other hand, for the OPO we have

$$\zeta = \frac{\eta}{\gamma}, \quad (A.3)$$

where η is the frequency-spreading between adjacent transverse modes in a Fabry-Perot with quasi-planar mirrors, and γ is the cavity linewidth. We want to show now that ζ for the OPO corresponds basically to α^{-2} for the OPA, so that increasing α in the OPA corresponds to decreasing ζ in the OPO.

For a quasi-planar cavity, one has

$$\eta \approx \frac{c}{z_0}, \quad (A.4)$$

where c is the light velocity in vacuum and z_0 is the Rayleigh range of the cavity. Because for a Fabry-Perot

cavity $\gamma = cT/(2L)$ where L is the cavity length, we have [22]

$$\zeta^{-1} = \frac{\gamma}{\eta} \approx \frac{z_0 T}{2L} = \frac{\pi w_0^2}{2\lambda L} T, \tag{A.5}$$

where w_0 is the beam waist, such that $z_0 = \pi w_0^2/\lambda$ [22]. Because the parameter w_0 in the OPO can be put in correspondence with $\sqrt{S_\mathrm{p}}$ in the OPA, one concludes that basically ζ^{-1} corresponds to α^2. The parameter T appears in (A.5) because of the presence of the mirrors in the OPO.

References

1. M.D. Reid, P.D. Drummond, Phys. Rev. Lett. **60**, 2731 (1988); Z.Y. Ou, S.F. Pereira, H.J. Kimble, Appl. Phys. B **55**, 265 (1992).
2. See *e.g.* C.H. Bennett, P.W. Shor, Science **284**, 747 (1999).
3. D. Bouwmeester, Jan-Wei Pan, K. Mattle, M. Eibl, H. Weinfurter, A. Zeilinger, Nature **390**, 575 (1997); S.L. Braunstein, H.J. Kimble, Phys. Rev. Lett. **80**, 869 (1998); D. Boschi, S. Branca, F. De Martini, L. Hardy, S. Popescu, Phys. Rev. Lett. **80**, 1121 (1998); A. Furusawa, J.L. Sorensen, S.L. Braunstein, C.A. Fuchs, H.J. Kimble, E.S. Polzik, Science **282**, 706 (1998).
4. L.A. Lugiato, M. Brambilla, A. Gatti, *Advances in Atomic, Molecular and Optical Physics*, edited by B. Bederson, H. Walther (Academic Press, Boston, 1999), Vol. 40.
5. M.I. Kolobov, Rev. Mod. Phys. **71**, 1539 (1999), and references quoted therein.
6. C. Fabre, J.B. Fouet, A. Maitre, Opt. Lett. **25**, 76 (2000).
7. M.I. Kolobov, C. Fabre, Phys. Rev. Lett. **85**, 3789 (2000).
8. B.M. Jost, A.V. Sergienko, A.F. Abouraddy, B.E.A. Saleh, M.C. Teich, Opt. Expr. **3**, 81 (1998).
9. I. Marzoli, A. Gatti, L.A. Lugiato, Phys. Rev. Lett. **78**, 2092 (1997).
10. A. Gatti, K.I. Petsas, I. Marzoli, L.A. Lugiato, Opt. Commun. **179**, 591 (2000); A. Gatti, L.A. Lugiato, K.I. Petsas, I. Marzoli, Europhys. Lett. **46**, 461 (1999); C. Swaj, G.L. Oppo, A. Gatti, L.A. Lugiato, Eur. Phys. J. D **10**, 433 (2000).
11. A. Gatti, E. Brambilla, L.A. Lugiato, M.I. Kolobov, Phys. Rev. Lett. **83**, 1763 (1999).
12. A. Gatti, E. Brambilla, M.I. Kolobov, L.A. Lugiato, J. Opt. B: Quant. Semiclass. Opt. **2**, 196 (2000).
13. G. Le Tolguenec, F. Devaux, E. Lantz, Opt. Lett. **24**, 1047 (1999); F. Devaux, E. Lantz, J. Opt. Soc. Am. B **12**, 2245 (1995).
14. M.L. Marable, S.-K. Choi, P. Kumar, Opt. Expr. **2**, 84 (1998); O. Aytür, P. Kumar, Phys. Rev. Lett. **83**, 1938 (1999)
15. M.I. Kolobov, L.A. Lugiato, Phys. Rev. A **52**, 4930 (1995).
16. I.V. Sokolov, M.I. Kolobov, L.A. Lugiato, Phys. Rev. A **60**, 2420 (1999).
17. A. Berzanskis, W. Chinaglia, L.A. Lugiato, K.H. Feller, P. Di Trapani, Phys. Rev. A **60**, 1626 (1999).
18. F. Devaux, E. Lantz, Eur. Phys. J. D **8**, 117 (1999).
19. M.I. Kolobov, I.V. Sokolov, Sov. Phys. JETP **69**, 1097 (1989); Phys. Lett. A **140**, 101 (1989).
20. R.J. Glauber, Phys. Rev. **130**, 2529 (1963).
21. S. Reynaud, C. Fabre, E. Giacobino, J. Opt. Soc. Am. B **4**, 1520 (1987).
22. A. Yariv, *Quantum Electronics*, 3rd edn. (Wiley, New York, 1989).